Design and Validation of a Self-Aligning Index Finger Exoskeleton for Post-Stroke Rehabilitation

Ning Sun, Guotao Li, and Long Cheng, *Senior Member, IEEE*

***Abstract*— Rehabilitation of hand functions is necessary to improve post-stroke patients' quality of life. There is initial evidence that hand exoskeletons should exercise flexion/extension (f/e) and abduction/adduction (a/a) of the fingers to rebuild hand functions. However, designing a self-alignment mechanism of the metacarpophalangeal (MCP) joint to improve its wearing comfort is still a challenge. In this paper, a novel index finger exoskeleton with three motors is proposed to help post-stroke patients perform finger a/a and f/e training. A spatial mechanism with passive degrees of freedom for the MCP joint is designed to realize human-robot axes self-alignment. The proposed mechanism's kinematic compatibility is analyzed to show its self-aligning capability, and the kineto-statics analysis is performed to present the exoskeleton's static characteristics. Finally, kinematic and static experiments have been conducted, and the results indicate that the standardized reaction forces square sum of the exoskeleton to the MCP joint can be reduced by 65.8% compared with the state-of-the-art exoskeleton. According to the experimental results, the exoskeleton can achieve the a/a and f/e training and human-robot axes self-alignment, and improve its comfortability. In the future, clinical trials will be further studied to test the exoskeleton.**

***Index Terms*— Finger exoskeleton, self-aligning mechanism, kinematic compatibility, kineto-statics.**

I. Introduction

LARGE numbers of people suffer from physical disorders due to stroke, such as hand dysfunction [1]. The loss of hand motor function reduces patients' self-care ability, leading to affect their quality of life [2]. Therefore, it is crucial to recover the patients' lost hand motor function. In general, hand rehabilitation training is performed by physical and occupational therapists [3]. However, some post-stroke patients, after discharge, cannot get timely and effective rehabilitation training due to the lack of therapists [3]. To solve these problems, hand exoskeleton robots are proposed to replace the therapists to assist post-stroke patients in rehabilitation training, such as repetition of simple grasp-release exercises [4], closing one or more fingers [5]. It has been verified that robot-aided hand therapy can improve hand motor function for post-stroke patients [4], [5].

Wearable exoskeleton robots for hand rehabilitation mainly include soft gloves and linkage-type exoskeletons. Popov *et al.* designed a portable exoskeleton glove developed for assistance in activities of daily living [6]. Yurkewich *et al.* developed a portable, lightweight hand extension robot orthosis glove to grasp everyday objects [7]. However, compared with the linkage-type exoskeletons, the soft gloves are difficult to ensure enough force for rehabilitation training [8]. Therefore, this paper focuses on the design of linkage-type exoskeletons.

Due to the complexity and the intersubjective variability of human finger skeletal kinematics, the human-exoskeleton axes self-alignment is a challenging task for the design of linkage-type exoskeletons [9]. Axes misalignment can produce undesired forces on the finger joints, resulting in damages to the users [9]. Therefore, the designers have to consider the human-exoskeleton joint axes misaligning problem when designing a hand exoskeleton. Li *et al.* designed an interactive hand exoskeleton by directly matching the device's joint axes and those of their corresponding finger joint [10]. Hong *et al.* designed an index finger exoskeleton by locating one side of the users' finger to align the rotation axes of joints [11]. Wang *et al.* proposed an underactuated linkage-slide mechanism to coincide with the human finger joints directly [12]. Ho *et al.* designed a circular orbital mechanism with virtual center to align the rotation axes of joints directly [13]. However, the axes of finger joints are variable because of the soft tissue of human finger joints or the intersubjective variability. The above devices cannot guarantee exoskeleton joint axes' self-aligning capability. Therefore, it still may cause inconvenience to the patients.

To guarantee the self-aligning capability of the exoskeletons, Jo *et al.* proposed a portable exoskeleton for exercising flexion/extension (f/e) of the fingers [14]. Solazzi *et al.*

Manuscript received December 28, 2020; revised April 14, 2021 and June 3, 2021; accepted June 28, 2021. Date of publication July 16, 2021; date of current version August 3, 2021. This work was supported in part by the Beijing Municipal Natural Science Foundation under Grant JQ19020 and in part by the National Natural Science Foundation of China under Grant 62025307 and Grant U1913209. *(Ning Sun and Guotao Li contributed equally to this work.) (Corresponding author: Long Cheng.)*

This work involved human subjects or animals in its research. Approval of all ethical and experimental procedures and protocols was granted by the Institute of Automation, Chinese Academy of Sciences under Approval No. IA-202044.

Ning Sun and Long Cheng are with the State Key Laboratory of Management and Control for Complex Systems, Institute of Automation, Chinese Academy of Sciences, Beijing 100190, China, and also with the School of Artificial Intelligence, University of Chinese Academy of Sciences, Beijing 100049, China (e-mail: long.cheng@ia.ac.cn).

Guotao Li is with the State Key Laboratory of Management and Control for Complex Systems, Institute of Automation, Chinese Academy of Sciences, Beijing 100190, China.

Digital Object Identifier 10.1109/TNSRE.2021.3097888

proposed an underactuated, linkage-based exoskeleton to perform grasping tasks [15]. This device can provide automatic adaptability for different finger sizes. Besides, linkage-type exoskeletons with flexible elements have been proposed to achieve self-alignment, where its joints corresponding to the finger joints use flexible elements. Bos *et al.* developed an electrohydraulic hand orthosis with flexure elements to assist hand functions [16]. The flexure elements can align the orthosis's rotational centers with those of the anatomical joints. Nycz *et al.* designed a hand exoskeleton using a three-layered sliding spring mechanism [17]. The bending shape of the multi-layered compliant mechanism can self-align to the anatomical joints' location. However, the above designs only assist the f/e motion of the finger.

Rehabilitation medicine studies indicate that occupational therapy can positively affect the recovery of upper extremities and hand functions [18]. Occupational therapy requires performing finger adduction exercise and finger abduction exercise [19]. Besides, rehabilitation of some fine motions such as turning knobs or handing chopsticks is necessary to improve the quality of life of post-stroke patients [20]. Therefore, the robotic device is required to assist not only the f/e motion but also the adduction/abduction (a/a) motion of the fingers.

To achieve the a/a motion, Agarwal *et al.* and Chiri *et al.* proposed a slider-crank-like index finger exoskeleton [21], [22]. In these designs, a passive degree-of-freedom (DOF) is used to allow the a/a motion of the metacarpophalangeal (MCP) joint. Ueki *et al.* and Wege *et al.* developed a double crank mechanism for the MCP joint [23], [24]. An active DOF in this design is added to achieve the a/a motion. However, the aforementioned devices cannot achieve human-exoskeleton axes self-alignment for the MCP joint. Cempini *et al.* developed a full self-alignment chain for the MCP joint [25]. This mechanism configuration with a cable-driven actuation system can achieve human-exoskeleton axes self-alignment and reduce the finger joints' reaction forces. However, this design assumes that the system's friction and other resistance forces are zero. In fact, it may result in large reaction forces to the MCP joint and shear force along with the phalanx, and mechanical stress exerted on finger joints causes degeneration and degenerative joint diseases [26]. Therefore, the self-alignment and comfort of the exoskeleton for the MCP joint need to be further studied.

The theoretical analysis method of self-alignment can help the design of hand exoskeletons. A kinematic compatibility analysis method is first proposed by Cempini *et al.* [9]. It proves the kinematic compatibility of planar mechanisms, such as the slider-crank-like mechanism. Furthermore, the kinematic compatibility of two DOFs self-aligning mechanism that can be decomposed into plane mechanisms has been analyzed. However, it does not presents the kinematic compatibility analysis of spatial mechanisms that could not be decoupled to planar mechanisms. Therefore, a kinematic compatibility analysis for the coupled spatial mechanism should be explored.

In this paper, a novel index finger exoskeleton is proposed to realize the a/a and f/e training of the finger. The contributions

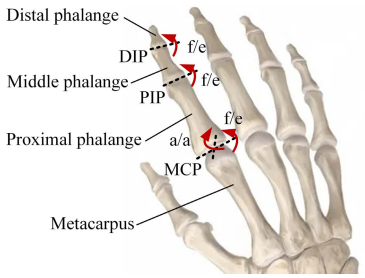

Fig. 1. The anatomy structure of the index finger.

of this paper can be summarized as follows: 1) An index finger exoskeleton is proposed based on a self-aligning spatial mechanism. The mechanism with passive DOFs can realize self-alignment. Three motors are used to complete the a/a and f/e training of the finger. 2) The proposed mechanism's kinematic compatibility is analyzed to show its self-aligning capability. 3) Considering friction and other system resistance forces, the mechanism can reduce the shear force and the reaction forces compared with the state-of-the-art exoskeleton in [8] and improve its wearing comfort.

The rest of this paper is organized as follows. In Section II, the index finger exoskeleton is designed and introduced. In Sections III and IV, the kinematic and kineto-statics models of the proposed spatial mechanism are established and analyzed. In Section V, experimental verifications are conducted. Section VI and VII give the discussion, conclusion, and future work.

II. Exoskeleton Design

A. Design Requirements

As shown in Fig. 1, the index finger consists of one metacarpus and three phalanges. It has three joints, including the MCP joint, proximal interphalangeal (PIP) joint, and distal interphalangeal (DIP) joint. The MCP joint is an ellipsoidal or condylar joint with ovoid-ellipsoid joint articulate surface shapes and can achieve the f/e and a/a motions. The PIP and DIP joints are bicondylar joints with double, ovoid joint articulate surface shapes and can achieve the f/e motion [27]. The motions of the PIP and DIP joints are coupled. This coupling relation still exists for post-stroke patients since it is determined by the interaction between the extrinsic and intrinsic musculature, while stroke only damages the sensory conduction pathway [28].

To guarantee rehabilitation performance, some relevant rehabilitation theories are summarized. The human upper limb studies have shown that breaking the complex motion into individual motion of each joint can achieve a better rehabilitation performance [29]. Besides, the relation between MCP and PIP joint angles of a finger is considerably variable in different grasping tasks [30]. Decomposing the MCP and PIP joints' synchronized motion into respective independent motions of each joint can rehabilitate multiple grasping tasks, such as larger diameter and lateral. Therefore, the f/e and a/a motions of the fingers should be controlled independently [31]. On the other hand, joint reaction forces in the translation directions may be generated by the exoskeletons, which burden

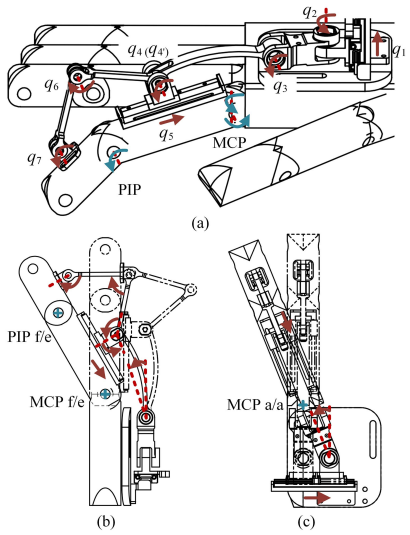

Fig. 2. Mechanism and its motions of the index finger exoskeleton. (a) Self-alignment Mechanism of the index finger exoskeleton. (b) The f/e motion of the MCP joint. (c) The a/a motion of the MCP joint.

the articulation [8]. According to [26], reducing the reaction forces should be among the design criteria. From the view of the wearability, the shear force along the finger phalanx causes an unstable connection between the exoskeleton and the fingers due to the skin's elasticity and softness, and it should be zero.

The index finger rehabilitation exoskeleton's design requirements in this paper can be summarized as follows. 1) It should consist of three motors to independently control each main DOF of the index finger MCP and PIP joints. 2) To verify the adaptability to different hand types, Pearson's product-moment correlation coefficients of joints motion trajectories without and with the exoskeleton for different subjects are larger than 0.6. 3) The shear force should almost be zero to avoid unstable connections. When the exoskeleton provides actuated torques to assist finger movement, low reaction forces in the translation directions should be satisfied even with the system's friction.

B. Mechanism Design

As shown in Fig. 2(a), the index finger's self-aligning mechanism was proposed to align the human-exoskeleton axes automatically. The mechanism configuration allows for the f/e and a/a motions of the MCP joint and the f/e motion of the PIP joint. The index finger is deemed a part of the whole mechanism. The index finger and the self-aligning mechanism together constitute two closed-loop mechanisms: MCP closed-loop chain and PIP closed-loop chain. Since the PIP and DIP joints' motions are coupled, the DIP joint's motion is not considered here. For the MCP closed-loop chain constituted by the MCP joint and corresponding links, if we simplify the MCP joint to a U kinematic pair (two intersecting R pairs), this mechanism can be deemed as a spatial mechanism, whose kinematic chain is P3RPU. The PIP closed-loop chain is constituted by the PIP joint and corresponding links, and can be deemed as a planar four-bar

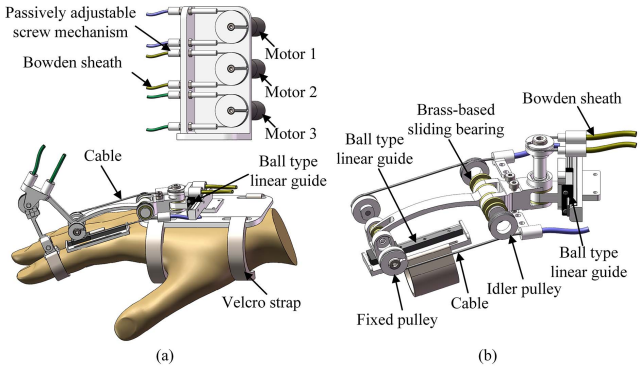

Fig. 3. CAD model of the index finger exoskeleton. (a) Overall design of index finger exoskeleton. (b) The exploded view of the MCP joint.

mechanism, whose kinematic chain is 4R since the position of the sliding joint q_5 has been determined by the MCP closed-loop chain.

To show clearly how the self-aligning mechanism actuates the f/e and a/a motions of the finger MCP joint, Fig. 2(b) and (c) depict the relative motion of each joint of the mechanism. The f/e motion of the MCP joint is realized by the revolute joints q_3, q_4, the sliding joint q_5 and the f/e motion axis of the MCP joint. If we assume the PIP joint is locked, the movement of the sliding joint q_5 causes relative motions of joints $q_{4'}$, q_6, and q_7 in the PIP closed-loop chain, as shown in Fig. 2(b). The a/a motion of the finger MCP joint is completed by the sliding joints q_1, q_5, the revolute joint q_2, q_3, q_4, and the a/a motion axis of the MCP joint. The relative motions of joints $q_{4'}$, q_6, and q_7 are also generated. From the analysis, it is obvious that the a/a and f/e motions of the MCP joint are coupled since the sliding joint q_5 is placed on the dorsum of the proximal phalanx. Although this design may bring some trouble to its kinematic relationship, it can ensure the only normal force on the finger phalanx.

C. Prototype

The index finger exoskeleton's overall design was implemented based on the self-aligning mechanism, which is shown in Fig. 3(a). To show its components clearly, Fig. 3(b) is depicted to give its exploded view. Two ball type linear guides are adopted as the sliding joints, which can reduce the mechanical system's friction. To reduce the structural volume, the brass-based sliding bearings are used to replace ball bearings in the revolution joints' design. The entire finger exoskeleton is grounded through the exoskeleton base, fixed on the wearer's hand with velcro straps, and the exoskeleton mechanism is also connected to the proximal and middle phalanges of the finger through velcro straps.

Three DC motors (Faulhaber1741T0012CXR with incremental encoder IEH2-4096, 50:1 planetary gearhead) are used as the exoskeleton's actuators, which can ensure that the f/e and a/a motions of the MCP and the f/e motion of the PIP are independently driven. Cable-driven systems are applied to reduce the weight and volume of the exoskeleton system, and all motors are placed outside the exoskeleton system.

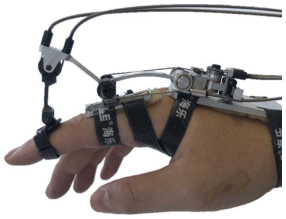

Fig. 4. Index finger exoskeleton prototype is worn on a subject's hand.

The cable-driven systems is composed of steel wires and flexible sheaths made of spiraled harmonic steel wire. All flexible sheaths are placed between the two fixed bases on the motor's end and the exoskeleton system's end. To keep the cable under tension, a passively adjustable screw mechanism is designed, which is connected with the flexible sheaths at the output end of the motors. The cables' ends are fixed to the pulleys at the motors' output ends. The other ends of the cables connected with motor 2 and 3 are directly fixed to the pulleys on the exoskeleton joints q_2 and q_6. Particularly, the other end of the cable connected with motor 1 is fixed to the exoskeleton joint q_4 through two pulleys. The first pulley placed on the revolute joint q_3 is idle, while the second pulley placed on the revolute joint q_4 is fixed with the corresponding link. The radii of the two pulleys are equal. This design can provide almost equal actuated torque on exoskeleton joints q_3 and q_4 according to [25]. The index finger exoskeleton prototype is fabricated based on the CAD model, as shown in Fig. 4.

III. Kinematics Analysis

A. Kinematic Compatibility Analysis

Human-exoskeleton joint axes misalignment generated by the soft tissue and intersubject variability may cause damage to human finger joints. Here, the MCP joint's misaligning displacements are modeled as three translations in three orthogonal directions [9]. The kinematics model of the human MCP joint shown in Fig. 5 is composed of two orthogonal rotations and three misaligning translations. How the proposed mechanism can automatically adjust itself to compensate the misaligning displacements of the MCP joint is analyzed here.

As shown in Fig. 5, the coordinate systems of the mechanism based on the D-H method are sequentially established along the exoskeleton chain and are expressed by the red arrow line. The D-H parameters of the exoskeleton kinematic chain are listed in Table I. The coordinate systems corresponding to two orthogonal rotations and three misaligning translations of the MCP joint are established based on the matrix transformation method and are expressed by the blue arrow line. In Fig. 5, V and H are the horizontal and vertical distances between the MCP joint and the first sliding joint of the exoskeleton chain. L_1, L_2, L_3, L_4 stand for the corresponding link length of the exoskeleton chain. L_5 is the distance between the sliding plane of the exoskeleton joint q_5 and the central axis of the proximal phalanx. L_6 is the distance between the MCP joint and the exoskeleton joint q_5 along the proximal phalanx in the extended state of the finger.

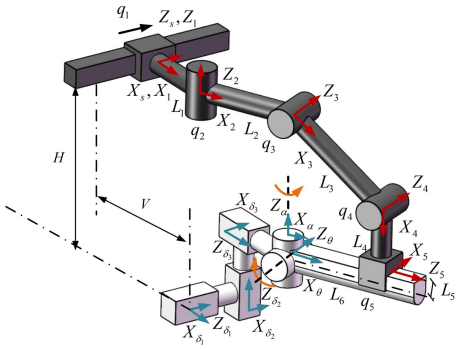

Fig. 5. The frame of the MCP exoskeleton kinematic chain and the MCP joint kinematic chain.

TABLE I
D-H Parameters of the MCP Exoskeleton Chain

i	α_{i-1}	a_{i-1}	d_i	θ_i
1	0	0	q_1	0
2	90	L_1	0	q_2
3	-90	L_2	0	q_3
4	0	L_3	0	q_4
5	90	L_4	0	90

Define the two orthogonal rotations of the MCP joint as $\tilde{q} = \begin{bmatrix} \theta & \alpha \end{bmatrix}^{\mathrm{T}}$, and define the misaligning displacements as $\delta = \begin{bmatrix} \delta_1 & \delta_2 & \delta_3 \end{bmatrix}^{\mathrm{T}}$. The kinematics of the closed-loop spatial mechanism can be expressed as

$$ {}^{s}_{e}T^{E}(q) = {}^{s}_{e}T^{H}(\tilde{q}, \delta), \tag{1} $$

where $q = \begin{bmatrix} q_1 & \dots & q_5 \end{bmatrix}^{\mathrm{T}}$ represents the angle or displacement variables of the exoskeleton joints, s represents a fixed global reference frame $(O_s - x_s, y_s, z_s)$, e represents the intersection coordinate system of the exoskeleton kinematic chain and the MCP joint kinematic chain. ${}^{s}_{e}T^{E}(q)$ represents the relative position and orientation of the coordinate system e and the reference frame s of the exoskeleton kinematic chain. ${}^{s}_{e}T^{H}(\tilde{q}, \delta)$ represents the relative position and orientation of the coordinate system e and the reference frame s of the MCP joint kinematic chain.

The left and right terms of Eq. (1) could be obtained by sequentially multiplying the homogeneous transformation matrices of adjacent coordinate systems along the exoskeleton kinematic chain and the MCP joint kinematic chain. Based on the D-H method, ${}^{s}_{e}T^{E}(q)$ expressed as

$$ {}^{s}_{e}T^{E}(q) = {}^{s}_{1}T^{1}_{2}T^{2}_{3}T^{3}_{4}T^{4}_{5(e)}T, \tag{2} $$

where

$$ {}^{i-1}_{i}T = \begin{bmatrix} {}^{i-1}_{i}R & {}^{i-1}_{i}P \\ 0 & 1 \end{bmatrix} $$

with ${}^{i-1}_{i}R$ and ${}^{i-1}_{i}P$ representing the rotation matrix and the translation vector, respectively. Based on the matrix transformation method, ${}^{s}_{e}T^{H}(\tilde{q}, \delta)$ can be expressed as

$$ {}^{s}_{e}T^{H}(\tilde{q}, \delta) = {}^{s}_{\delta_1}T^{\delta_1}_{\delta_2}T^{\delta_2}_{\delta_3}T^{\delta_3}_{\alpha}T^{\alpha}_{\theta}T^{\theta}_{5(e)}T, \tag{3} $$

where

$$ {}^{s}_{\delta_1}T = \begin{bmatrix} 1 & 0 & 0 & V \\ 0 & 1 & 0 & H \\ 0 & 0 & 1 & \delta_1 \\ 0 & 0 & 0 & 1 \end{bmatrix}, \quad {}^{\delta_1}_{\delta_2}T = \begin{bmatrix} 0 & -1 & 0 & 0 \\ 0 & 0 & -1 & -\delta_2 \\ 1 & 0 & 0 & 0 \\ 0 & 0 & 0 & 1 \end{bmatrix}, $$

$$ {}^{\delta_2}_{\delta_3}T = \begin{bmatrix} 1 & 0 & 0 & 0 \\ 0 & 0 & -1 & -\delta_3 \\ 0 & 1 & 0 & 0 \\ 0 & 0 & 0 & 1 \end{bmatrix}, \quad {}^{\delta_3}_{\alpha}T = \begin{bmatrix} \sin\alpha & \cos\alpha & 0 & 0 \\ 0 & 0 & 1 & 0 \\ \cos\alpha & -\sin\alpha & 0 & 0 \\ 0 & 0 & 0 & 1 \end{bmatrix}, $$

$$ {}^{\alpha}_{\theta}T = \begin{bmatrix} \cos\theta & -\sin\theta & 0 & 0 \\ 0 & 0 & 1 & 0 \\ -\sin\theta & -\cos\theta & 0 & 0 \\ 0 & 0 & 0 & 1 \end{bmatrix}, $$

$$ {}^{\theta}_{5(e)}T = \begin{bmatrix} 0 & 0 & 1 & L_6+q_5 \\ 0 & -1 & 0 & -L_5 \\ 1 & 0 & 0 & 0 \\ 0 & 0 & 0 & 1 \end{bmatrix}. $$

Substituting the results of Eqs. (2) and (3) into Eq. (1) yields

$$ \begin{pmatrix} \theta \\ \alpha \\ \delta_1 \\ \delta_2 \\ \delta_3 \end{pmatrix} = \begin{pmatrix} q_3+q_4-\pi/2 \\ q_2 \\ q_1+((L_4+L_5)c_{34}+L_2+L_3c_3-(L_6+q_5)s_{34})s_2 \\ H-(L_6+q_5)c_{34}-(L_4+L_5)s_{34}-L_3s_3 \\ L_1-V+(L_2+(L_4+L_5)c_{34}+L_3c_3-(L_6+q_5)s_{34})c_2 \end{pmatrix}, \tag{4} $$

where θ and α stand for the angles of f/e and a/a motions of the MCP joint, respectively. $\delta_1, \delta_2, \delta_3$ stand for the misaligning displacements of human-robot axes, and there are $s_i = \sin q_i$, $c_i = \cos q_i$, $s_{ij} = \sin(q_i + q_j)$, $c_{ij} = \cos(q_i + q_j)$ $(i, j = 2, 3, 4)$.

This result indicated that any position (θ, α, and δ_1, δ_2, δ_3) of the MCP joint could be absorbed through the exoskeleton kinematic chain. In other words, the proposed mechanism for the MCP joint is compatible with the kinematics of the human finger joint.

B. Forward Kinematics

According to Eq. (4), it is obvious that the a/a motion angle α of the MCP joint is only related to the exoskeleton joint q_2, which can be expressed as

$$ \alpha = q_2. \tag{5} $$

While the f/e motion angle θ of the MCP joint is related to multiple joints of the exoskeleton, the f/e motion angle θ can be calculated based on Eq. (4). Eq. (4) can be transformed into

$$ A\cos\theta + B\sin\theta - C = 0, \tag{6} $$

where $A = (H-\delta_2)c_2 - L_3s_3c_2$, $B = (L_1 - V - \delta_3) + L_2c_2 + L_3c_3c_2$, $C = (L_4 + L_5)c_2$.

TABLE II
THE PARAMETERS OF THE PROPOSED MECHANISM

L_1	10.5mm	L_2	20.5mm
L_3	45mm	L_4	8.6mm
L_5	13.2mm	L_6	36mm
H	22mm	V	39mm
q_2	$0 \sim 35°$	q_3	$-10 \sim 60°$

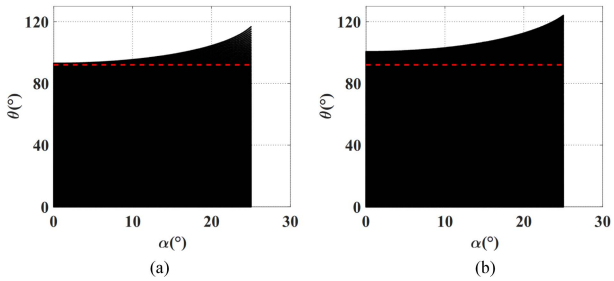

Fig. 6. The workplaces of the MCP joint with the index finger exoskeleton. (a) The misaligning displacements are all 0mm. (b) The misaligning displacements are 5mm, 5mm, 4mm, respectively.

By using the universal formula of trigonometric function, Eq. (6) can be transformed into

$$ (A+C)t^2 - 2Bt + C - A = 0, \tag{7} $$

where $t = \tan(\theta/2)$.

Solving Eq. (7) yields

$$ \theta = 2\arctan\left(\frac{D-\sqrt{D^2+((H-\delta_2-L_3s_3)^2-(L_4+L_5)^2)c_2^2}}{(H-\delta_2-L_3s_3+L_4+L_5)c_2}\right), \tag{8} $$

where $D = L_1 - V - \delta_3 + L_2c_2 + L_3c_3c_2$.

The angles of the MCP f/e and a/a motions can be obtained according to Eqs. (5) and (8), determined by the angles of the exoskeleton joints q_2 and q_3. The forward kinematics of the PIP closed-loop chain is described in Appendix.

C. Workplace Analysis

The maximum range of f/e and a/a motions of the index finger MCP joint are 92° and 24°, respectively [10]. The proposed mechanism should help the MCP joint reach all-natural movement positions. The workplace where the mechanism assists the MCP joint movement is obtained according to Eqs. (5) and (8), and it is related to link lengths of the exoskeleton, the misaligning displacements, and the ROM of the joints q_2, q_3. Link lengths of the exoskeleton and the ROM of the joints are shown in Table II. It is difficult to estimate the misaligning displacements due to the intersubject variability of human skeletal kinematics. For simplicity, we preset the misaligning displacements $\begin{bmatrix}\delta_1 & \delta_2 & \delta_3\end{bmatrix}^{\mathrm{T}}$ to $\begin{bmatrix}0 & 0 & 0\end{bmatrix}^{\mathrm{T}}$mm and $\begin{bmatrix}5 & 5 & 4\end{bmatrix}^{\mathrm{T}}$mm. Fig. 6(a) and (b) represent the workplaces of the f/e and a/a motions of the MCP joint under the different value of the misaligning displacements. The red dotted line stands for the maximum range of f/e motion. Therefore, the maximum motion angle of the MCP joint can be reached.

IV. Kineto-Statics Analysis

A. Kineto-Statics Modeling

Differentiating Eq. (4) yields

$$\dot{\Theta} = J(q)\dot{q}, \tag{9}$$

where $\dot{\Theta}$ stands for the velocity vector of the MCP joint, $\dot{q}$ represents the velocity vector of the exoskeleton joints, and $J(q)$ stands for the Jacobian matrix of the exoskeleton system. The expression of $J(q)$ can be calculated by the symbolic computation in MATLAB.

Based on the virtual work principle, there is

$$\tau_q = J^{\mathrm{T}}(q)\tau_\Theta, \tag{10}$$

where $\tau_\Theta = \begin{bmatrix} \tau_\theta & \tau_\alpha & \tau_{\delta_1} & \tau_{\delta_2} & \tau_{\delta_3} \end{bmatrix}^{\mathrm{T}}$ represents the forces/torques of the MCP joint. τ_θ and τ_α are the actuated torques applied in the f/e and a/a motion, respectively. τ_{δ_1}, τ_{δ_2}, τ_{δ_3} stand for the joint reaction forces applied in the misaligning directions. $\tau_q = \begin{bmatrix} \tau_{q_1} & \tau_{q_2} & \tau_{q_3} & \tau_{q_4} & \tau_{q_5} \end{bmatrix}^{\mathrm{T}}$ represents the forces/torques of the exoskeleton joints. Eq. (10) can be rewritten as

$$\begin{pmatrix} \tau_{q_1} \\ \tau_{q_2} \\ \tau_{q_3} \\ \tau_{q_4} \\ \tau_{q_5} \end{pmatrix} = \begin{pmatrix} \tau_{\delta_1} \\ \tau_\alpha + \tau_{\delta_1} M c_2 - \tau_{\delta_3} M s_2 \\ \tau_\theta + \tau_{\delta_1} N s_2 + \tau_{\delta_2}(I - L_3 c_3) + \tau_{\delta_3} N c_2 \\ \tau_\theta + (N + L_3 s_3)(\tau_{\delta_1} s_2 + \tau_{\delta_3} c_2) + \tau_{\delta_2} I \\ -\tau_{\delta_1} s_{34} s_2 - \tau_{\delta_2} c_{34} - \tau_{\delta_3} s_{34} c_2 \end{pmatrix}, \tag{11}$$

where $M = (L_4 + L_5)c_{34} + L_2 + L_3 c_3 - (L_6 + q_5)s_{34}$, $N = -(L_4 + L_5)s_{34} - L_3 s_3 - (L_6 + q_5)c_{34}$, $I = (L_6 + q_5)s_{34} - (L_4 + L_5)c_{34}$.

To avoid the reaction forces of the MCP joint in the translation directions, the forces in the misaligning directions should be null. That is, $\tau_{\delta_1} = \tau_{\delta_2} = \tau_{\delta_3} = 0$. By substituting $\tau_{\delta_1} = \tau_{\delta_2} = \tau_{\delta_3} = 0$ into Eq. (11), the output forces/torques of the exoskeleton joints are obtained as

$$\tau_{q_1} = \tau_{q_5} = 0, \quad \tau_{q_3} = \tau_{q_4} = \tau_\theta, \quad \tau_{q_2} = \tau_\alpha. \tag{12}$$

The first term $\tau_{q_1} = \tau_{q_5} = 0$ can be ensured since joints q_1, q_5 are passive sliding joints. The second and three terms in Eq. (12) can also be ensured by choosing the appropriate actuators. The study in [25] has proven that the same torque on the exoskeleton joints q_3 and q_4 can be generated by the cable-driven system shown in Fig. 3(b). For details, refer to ref. [25]. Thus, $\tau_{q_3} = \tau_{q_4} = \tau_\theta$ holds. In a word, the design in this paper is beneficial for eliminating the joint reaction forces exerted on the MCP joints by the exoskeleton. However, this result can be guaranteed only when the system's friction and other resistance forces are not considered.

B. Reaction Force to the MCP Joint

Due to friction and other resistance forces, transmission loss in the mechanical system makes the input torque of some joints unequal, which may cause that the joint reaction forces cannot be null. This case is analyzed in this part. Assume that the input torques difference of the exoskeleton joints q_3 and q_4 is δT and there exists

$$\tau_{q_4} = \tau_{q_3} - \delta T. \tag{13}$$

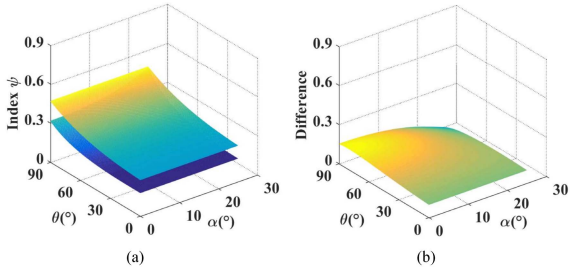

Fig. 7. RFSS distribution. (a) RFSS with the f/e and a/a motions, the lower one is the RFSS of the proposed exoskeleton, and the higher one is that of the exoskeleton in [8]. (b) Comparison of RFSS between the existing and proposed scheme.

Substituting Eq. (13) into Eq. (11) yields

$$\begin{cases} \tau_{\delta_1} = 0, \\ \tau_{\delta_2} = -\delta T s_{34}/(L_3 s_4), \\ \tau_{\delta_3} = \delta T c_{34}/(L_3 s_4 c_2). \end{cases} \tag{14}$$

Similarly, for the index finger exoskeleton proposed in [8], define the torques difference of the two joints connected with the cable as δT. Based on the torque difference, the reaction forces can be obtained as

$$\begin{cases} \tau_{\delta_1} = 0, \\ \tau_{\delta_2} = -\delta T/(L_3 c_4), \\ \tau_{\delta_3} = 0. \end{cases} \tag{15}$$

To give a quantitative analysis, two performance indexes of the finger exoskeleton are defined here: a standardized reaction forces square sum (SRFSS) and an absolute value of force along with finger phalanx (AFFP).

1) SRFSS: This performance index can be expressed as

$$\Lambda = \left(\frac{\int\int \psi d\alpha d\theta}{\int\int d\alpha d\theta}\right)^{1/2}. \tag{16}$$

where $\psi = \tau_{\delta_1}^2 + \tau_{\delta_2}^2 + \tau_{\delta_3}^2$ represents the reaction forces square sum (RFSS), $\tau_{\delta_i}(i = 1, 2, 3)$ can be calculated based on Eqs. (14) and (15). Assume that $\delta T = 0.019$Nm, the RFSS distribution on the workplaces of the MCP joint can be calculated and depicted in Fig. 7. Compared with the state-of-the-art exoskeleton in [8], the RFSS of the proposed scheme is lower in any position. Further, the SRFSS values for the proposed device and the device in [8] are calculated, and they are 0.470N and 0.584N, respectively. Compared with the exoskeleton in [8], the SRFSS is reduced by 19.5%.

2) AFFP: This performance index can be expressed as

$$\sigma_P = |\tau_{\delta_3} c_2 c_\theta - \tau_{\delta_2} s_\theta|, \tag{17}$$

where $s_\theta = \sin\theta$, $c_\theta = \cos\theta$. Fig. 8 shows the AFFP with the change of the f/e motion angle θ for the proposed finger exoskeleton and the existing one in [8]. It can be seen that the AFFP for the proposed finger exoskeleton is null, while the AFFP for the existing one is not zero and increases with the variation θ.

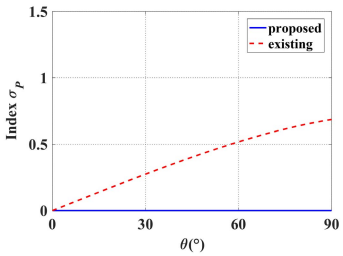

Fig. 8. AFFP with the change of the f/e motion angle.

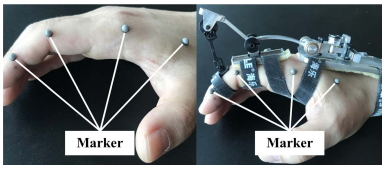

Fig. 9. Experimental setup of the index finger exoskeleton with the motion capture markers.

V. Experimental Validation

In this section, experiments were conducted to achieve four objectives: 1) to evaluate the kinematic transparency of the device, i.e., whether it affects the finger natural movement significantly and achieves the adaptability to different hand types; 2) to assess the a/a and f/e training capability of the exoskeleton; 3) to validate the accuracy of kinematics analysis and the self-aligning performance of the proposed spatial mechanism; 4) to evaluate comfort by the amount of the joint reaction forces and the shear force.

A. Kinematic Transparency

In the first experiment, the developed exoskeleton's kinematic transparency tests were performed with and without the exoskeleton to quantify the similarity of finger joints motions and evaluate the adaptability to different hand types. A motion capture system (Prime 13, OptiTrack, USA) equipped with eight high-speed cameras was used to record the index finger joints' motion data. The system's sampling frequency is 180 Hz, and the average accuracy of reconstructed marker coordinates is 0.17mm. As shown in Fig. 9, four markers were placed on the index finger's one side: three markers on the DIP, PIP, and MCP joints outside and one on the hand's dorsal shell, proximal to the thumb, which can avoid some possible interferences with the exoskeleton.

Six subjects with different hand types have been recruited according to their gender, age, weight, and height. They volunteer to participate in the experiment and sign an informed consent. This experiment is permitted by the Institute of Automation Chinese Academy of Sciences on April 5, 2020 (IA-201931). Six subjects are five males and one female. The subjects' age, weight, and height are 25-35 years old, 54-115 kg, and 162-185 cm, respectively. Each subject performed three movements in two different modes: a) NA: subjects actively performed movements without the index finger exoskeleton; b) NE: subjects wore the exoskeleton and actively performed movements. The following three different motions were performed: 1) full f/e motion of the MCP, PIP, and DIP joints without the a/a motion of the MCP joint; 2) full a/a motion of the MCP joint without the f/e motion of the MCP, PIP, and DIP joints; 3) hand fully closed and opened, including the f/e motion of the MCP, PIP, and DIP joints and the a/a motion of the MCP joint. Each motion was repeated three times. Note that the thumb maintains a constant posture during various motions to avoid its influence on motion data.

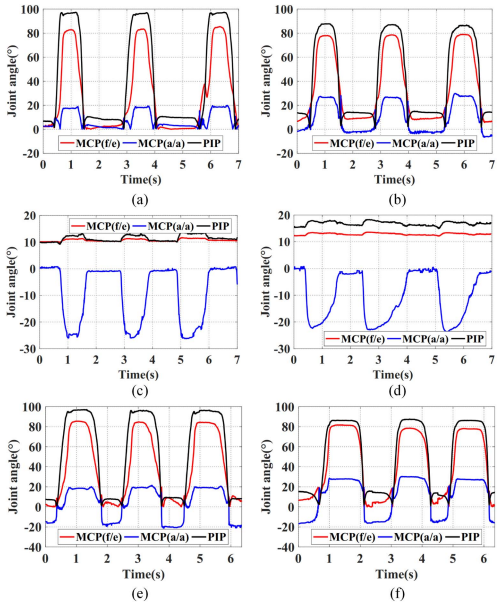

Fig. 10. Trajectories for subject #1 in NA and NE modes. The left and right columns are the plots of the finger joint angles without and with the finger exoskeleton, respectively. (a) and (b) represent the first motion, (c) and (d) represent the second motion, (e) and (f) represent the third motion.

TABLE III
Pearson's Product Moment Correlation Coefficients Averaged Over Three Repetitions for Six Subjects

	Subj.#1	Subj.#2	Subj.#3	Subj.#4	Subj.#5	Subj.#6
$r_p(\theta_{\mathrm{MCP}})$	0.939	0.910	0.907	0.937	0.962	0.926
$r_p(\alpha_{\mathrm{MCP}})$	0.903	0.886	0.813	0.847	0.766	0.823
$r_p(\theta_{\mathrm{PIP}})$	0.982	0.941	0.925	0.962	0.985	0.931

Based on the motion data recorded by the motion capture system, the index finger joints' angles can be obtained: the angles of the MCP and PIP f/e motions and the angle of the MCP a/a motion. For simplicity, the motion results for one in six subjects are reported, and the trajectories for Subj. #1 in two modes are shown in Fig. 10. The level of similarity of finger joints motion in NE and NA modes is evaluated by calculating Pearson's product-moment correlation coefficients. The coefficients are obtained based on the motion data of the third movement. Table III reports the Pearson's product-moment correlation coefficients averaged over three repetitions for six subjects. Among the six subjects, the average correlation values of MCP f/e, a/a, and PIP f/e motion trajectories are 0.930, 0.840 and 0.954, respectively. The results show a strong correlation between the joint angle trajectories in the two modes. The proposed exoskeleton has no significant effect on the index finger's natural movement with different hand types. Therefore, it can adapt to different hand types.

TABLE IV
ROM RESULTS OF TWO SUBJECTS WITHOUT AND WITH THE EXOSKELETON

Subject	Joint	Active ROM				Passive ROM	
		Without		With		With	
		Flexion	Extension	Flexion	Extension	Flexion	Extension
Subj.#1	MCP a/a	26.1°	0°	23.7°	0°	19.7°	0.8°
	MCP f/e	85.4°	0°	80.4°	0°	77.1°	1.2°
	PIP f/e	97.4°	0°	87.3°	0.5°	84.6°	0.4°
Subj.#2	MCP a/a	33.3°	0°	29.5°	0°	20.4°	0.5°
	MCP f/e	84.4°	0°	81.4°	0.5°	78.7°	1.6°
	PIP f/e	101.4°	5.7°	87°	5.2°	85.9°	2°

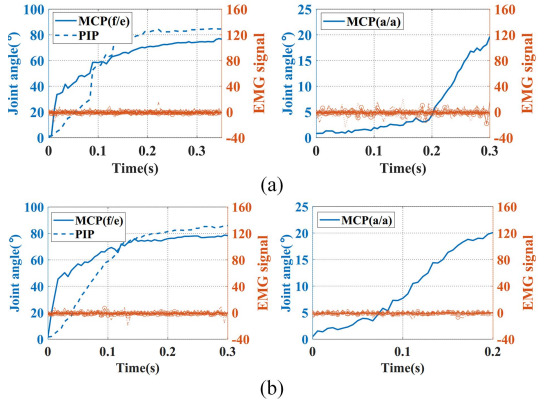

Fig. 11. The passive ROM of finger joints driven by the exoskeleton and the surface EMG signal. (a) Subject #1; (b) Subject #2.

B. Flexion/Extension-Adduction/Abduction Training Ability

In this experiment, the f/e and a/a training capability of the exoskeleton is evaluated by measuring the ROM of finger joints. The ROM of finger joints is affected by the device's relative attachment to the subjects' fingers. To show its influence, the finger joints' active ROM is obtained according to the first two movements on the kinematic transparency tasks. Table IV presents the active ROM results for subject #1 and subject #2. The results show that the finger joints' active ROM is reduced when the proposed index finger exoskeleton is attached to the subjects' hand.

Then, the test of the exoskeleton driving the human hand was performed. The cable-driven systems were installed, and the exoskeleton was worn on the subjects' index finger, assisting the index finger to perform the f/e and a/a motions. An MYO armband developed by Thalmic Labs, Canada was worn on the subjects' arms to collect the surface EMG signals that control finger movement. Four markers were placed on the index finger's side to obtain the index finger joints' angle. Fig. 11 shows the passive ROM of the finger joints and the surface EMG signal during the f/e and a/a motions. The passive ROM is also shown in Table IV. The surface EMG signals are constant, so there is no active movement of the index finger. The passive ROM is slightly smaller than the active ROM. The cable-driven systems can affect the ROM of finger joints. However, rehabilitation training can still be performed.

C. Kinematic Model and Self-Aligning Performance Validation

The kinematic model and self-aligning performance of the proposed mechanism are verified here. A fake finger with the same DOFs as a human index finger has been designed and used in this test. The MCP f/e and a/a motions and the PIP f/e motion were performed simultaneously. The angles of the MCP and PIP joints and exoskeleton joints q_2, q_3, q_6 were obtained through the motion capture system. The comparison of the MCP and PIP joints angle trajectories calculated through exoskeleton joints q_2, q_3, q_6 and those obtained through motion capture data directly are depicted in Fig. 12(a). It can be seen easily that the calculated angle is roughly consistent with the measured angle.

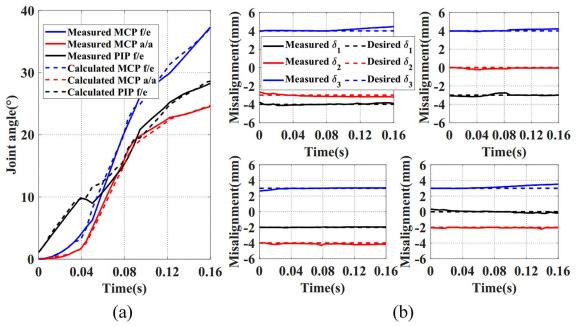

Fig. 12. Comparison of the angles of the MCP and PIP joints and the misaligning displacements. (a) The MCP and PIP joints angle trajectories. (b) The misaligning displacements.

To verify the self-aligning performance, the misaligning displacements $[\delta_1 \ \delta_2 \ \delta_3]^T$ of the MCP joint are set to $[-4 \ -3 \ 4]^T$, $[-3 \ 0 \ 4]^T$, $[-2 \ -4 \ 3]^T$, and $[0 \ -2 \ 3]^T$mm, respectively. The MCP f/e and a/a motions were performed simultaneously. The angles of the exoskeleton joints q_2, q_3, q_4 and the displacements of the exoskeleton joints q_1, q_5 were obtained through the motion capture system to calculate the compensation displacements. The compensation displacements for different misaligning displacements are shown in Fig. 12(b). The exoskeleton joints can compensate for the misaligning displacements of the MCP joint. Therefore, the proposed mechanism can realize human-robot axes self-alignment. The fluctuation in Fig. 12 is generally related to the marker and system shock position.

D. Evaluation of the Joint Reaction Forces and the Shear Force

The exoskeleton's comfort is evaluated by measuring the joint reaction forces and the shear force. Based on the fake finger shown in Fig. 13, an experiment platform was designed. The MCP angle of a/a motion α is set to zero here. The index finger exoskeleton assisted the phalanx to perform the MCP joint flexion motion at low speed (motor speed 1.6 r/min). Two flexible force sensors were placed on the proximal phalanx's back and front, respectively. No flexible force sensor was installed in other directions since the force τ_y perpendicular to the finger phalanx in the horizontal plane can be ignored during the flexion motion. The interaction forces on the finger phalanx are measured. The shear force τ_x along the finger phalanx can be obtained according to the sensor placed on the front of the proximal phalanx. Fig. 14(a) shows the relation between the shear force and the flexion motion's angle θ, which indicates that the shear force is closed to zero.

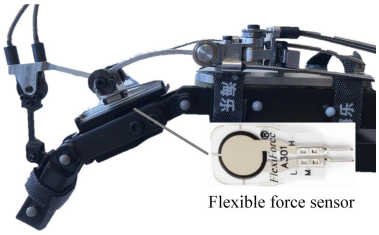

Fig. 13. Experimental platform for evaluating the joint reaction forces.

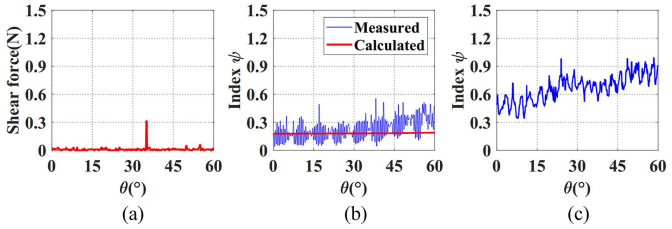

Fig. 14. The shear force and the reaction forces. (a) The shear force in flexion motion. (b) The joint reaction forces generated by the index finger exoskeleton. (c) The joint reaction forces generated by the mechanism configuration in [8].

It is difficult to directly measure the joint reaction forces exerted on the MCP joints. Therefore, the interaction forces are used to estimate the reaction forces according to the statical equilibrium of the phalanx. The dynamic effect could be neglected due to the finger phalanx's low motion speed. The reaction forces can be obtained as

$$\begin{cases} \tau_{\delta_1} = \tau_x s_\alpha + \tau_y c_\alpha, \\ \tau_{\delta_2} = -\tau_x s_\theta c_\alpha + \tau_y s_\theta s_\alpha + \tau_z c_\theta, \\ \tau_{\delta_3} = \tau_x c_\theta c_\alpha - \tau_y c_\theta s_\alpha + \tau_z s_\theta, \end{cases} \tag{18}$$

where τ_z is the force perpendicular to the finger phalanx in the vertical plane, and $s_\alpha = \sin\alpha$, $c_\alpha = \cos\alpha$. The RFSS value can be obtained as

$$\psi = \tau_{\delta_1}^2 + \tau_{\delta_2}^2 + \tau_{\delta_3}^2 = \tau_z^2. \tag{19}$$

Based on the measured values through the flexible force sensor, the RFSS ψ can be obtained through Eqs. (18) and (19). The RFSS value calculated by Eq. (14) in Section IV is also obtained. The two results are depicted in Fig. 14(b), from which it can be seen that the calculated RFSS approximately coincides with the measured one. In addition, an experiment platform based on the mechanism configuration in [8] has been designed and fabricated, and the joint reaction forces to the MCP joint have been measured by using the same method. The results are depicted in Fig. 14(c). The SRFSS values for the proposed device and the mechanism configuration in [8] are calculated by trapezoidal numerical integration, and they are 0.227N and 0.664N, respectively. The SRFSS is reduced by 65.8% compared with the mechanism configuration in [8]. In a word, the proposed exoskeleton can produce low reaction forces and shear force on the fingers and improve comfort. The difference between the experimental and simulation results may be caused by the friction inconsistency, the test platform's manufacturing errors, and links elasticity. It appears some fluctuations in the measured value. The reasons can be summarized as follows: the artificial finger's manufacturing errors, such as the gap between the phalanx and exoskeleton, poor contact, and the elastic force sensors' measurement errors.

TABLE V
COMPARISON WITH OTHER HAND REHABILITATION EXOSKELETONS

	Active movement	Self-alignment	Comfort	
			Shear force	Reaction forces (*N*)
Ueki [23]	f/e, a/a	×	Y	–
Wang [12]	f/e	×	Y	–
Bos [16]	f/e	×	N	–
Agarwal [21]	f/e	×	N*	–
Chiri [22]	f/e	×	N*	–
Cempini [8]	f/e	√	Y	0.664
Proposed device	f/e, a/a	√	N	0.227

Y indicates that there is shear force, which may cause skin injuries; N indicates there is no shear force; * represents that the shear force may be produced in the f/e motion due to axes misalignment.

VI. DISCUSSION

In this paper, a novel index finger exoskeleton has been proposed to realize the f/e and a/a training. Table V lists the comparison with some typical rehabilitation hands. Many hand exoskeletons cannot realize human-exoskeleton axes self-alignment for the MCP joint. Although a sliding joint can eliminate the shear force in the design proposed by Agarwal *et al.* or Chiri *et al.*, it may still be produced in the f/e motion since axes misalignment may limit the relative movement of the sliding joint. The device proposed in this paper and the design proposed by Cempini *et al.* can achieve human-exoskeleton axes self-alignment for the MCP joint. However, the kineto-statics analysis results indicate that there is the shear force in the design proposed by Cempini *et al.* and it increases with the increase of the flexion angle. Besides, the SRFSS values for the proposed device and the mechanism configuration in [8] are 0.227N and 0.664N, respectively. Compared with the mechanism configuration in [8], the SRFSS is reduced by 65.8%. Therefore, the proposed mechanism can improve comfort.

The kinematic compatibilities of planar mechanisms and decoupled spatial mechanisms have been analyzed in previous studies. In this paper, the kinematic compatibility of the MCP joint's coupled spatial mechanism has been further analyzed. This work can extend the kinematic compatibility analysis method. The exoskeleton's kinematic compatibility has been verified by the kinematic experiment. It is worth noting that the exoskeleton links length should be selected reasonably to compensate for the proximal shifting of the joint q_5 caused by the increased abduction angle. The Pearson's product-moment correlation coefficients of MCP f/e, a/a, and PIP f/e motion trajectories averaged for all subjects are 0.930, 0.840, and 0.954, respectively, and these results can verify the kinematic transparency of the mechanism. According to the finger joints' ROM with and without the exoskeleton, the exoskeleton's relative attachment to the finger phalanges affects the achievable range of the finger joints. Therefore, different finger ROM regions can be exercised by adjusting the exoskeleton attachment relative to the finger. The same result is also confirmed by reference [21].

The PIP closed-loop chain's DOF is 1 since the sliding joint position q_5 has been determined by the MCP closed-loop chain mechanism. The PIP joint angle can then be obtained based on the revolute joint q_6 in theory. The revolute joint angle q_6 can be measured by the encoder placed on the motor's end. However, there are some uncertainties in the PIP joint position due to the wearing position's uncertainty. The PIP closed-loop chain may extend quite high above the fingers to obtain a large PIP joint ROM. This makes some tasks difficult to achieve due to the possible collision between the exoskeleton and external objects. The cable-driven systems are applied to reduce the weight and volume of the exoskeleton. The exoskeleton joints q_3, q_4 are driven together by a single cable wrapped around two equal pulleys to eliminate the reaction forces. This design has also been applied in reference [9]. However, the system's friction and other resistance forces may cause unequal torque in the two exoskeleton joints, leading to the reaction forces. The cable may limit the user's finger motion range and arm movement due to large obstructive forces caused by exceeding the cable's maximum length or gravity.

The reaction forces and the shear force are obtained by measuring the exoskeleton's interaction forces and an artificial finger. Experimental results prove the exoskeleton's wearing comfort. Although the exoskeleton is worn on an artificial finger instead of a human finger, the actual reaction forces and the shear force on the human finger are still reflected based on the MCP closed-loop chain's kinematic and kineto-static relations. For example, in reference [14], the joint moments between the exoskeleton and the finger are measured by a fake hand. Although an estimating method for the human joint's undesired translational forces has been proposed in [22], this method is still hard to estimate the human joint's undesired translational forces when wearing other finger exoskeletons. Therefore, a fake finger is used in this paper to obtain the reaction forces' distribution to the MCP joint.

In the future, we will propose a calibration method to obtain the PIP closed-loop chain's accurate kinematics model, which will help control the PIP joint's position in practice. Also, post-stroke patients will be recruited, and a large number of clinical trials and measurements will be carried out. These clinical trials would offer further insight into the f/e and a/a training capability, the self-aligning capability, and comfortability.

VII. Conclusion

In this paper, an index finger exoskeleton was designed for post-stroke patients. A spatial mechanism with passive DOFs has been proposed to achieve self-alignment. Its kinematic compatibility was analyzed to prove its self-aligning capability, and the mechanism's kineto-statics was studied to present the exoskeleton's static characteristics. Finally, the kinematic and static experiments were conducted, and the results show that the coefficients of MCP f/e, a/a, and PIP f/e motion trajectories averaged for all subjects are 0.930, 0.840, and 0.954, respectively, which can verify the kinematic transparency of the mechanism. Besides, the SRFSS is reduced by 65.8% compared with the mechanism configuration in [8]. The theoretical analysis and experimental results indicate that the exoskeleton can realize the f/e and a/a training and human-exoskeleton axes self-alignment, and improve its comfortability.

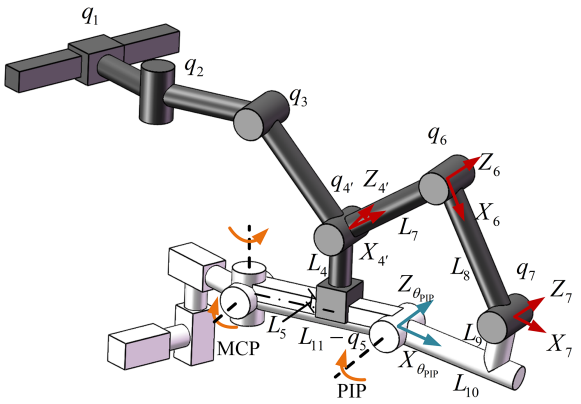

Fig. 15. The kinematic model of the PIP closed-loop chain.

Appendix
Forward Kinematics of the PIP Closed-Loop Chain

The kinematic model of the PIP closed-loop chain is shown in Fig. 15, and its coordinate systems are established based on the matrix transformation method. L_7, L_8 stand for the corresponding link length of the exoskeleton. L_9 is the distance between the revolute joint q_7 and the central axis of the middle phalanx. L_{10} stands for the distance between the PIP joint and the connection point of the exoskeleton and the middle phalanx. L_{11} is the distance between the PIP joint and the exoskeleton joint q_5 along the proximal phalanx in the extended state of the finger. The product of all homogeneous matrices is equal to an identity matrix I_4 since the chain is a single closed-loop mechanism. The kinematics of the PIP closed-loop chain can be expressed as

$$ {}^{PIP}_{4'}T\,{}^{4'}_{6}T\,{}^{6}_{7}T\,{}^{7}_{PIP}T = I_4. \tag{20}$$

Solving Eq. (20) yields

$$\theta_{PIP} = \arccos\left(\frac{E + L_{10}^2 + L_9^2 - L_7^2 - L_8^2 - 2L_7L_8\cos q_6}{2\sqrt{E}\sqrt{L_9^2 + L_{10}^2}}\right) + \arctan\left(\frac{L_4 + L_5}{L_{11} - q_5}\right) + \arctan\left(\frac{L_9}{L_{10}}\right) - \pi, \tag{21}$$

where $E = (L_4 + L_5)^2 + (L_{11} - q_5)^2$. The angle of the PIP f/e motion can be obtained according to Eq. (21), determined by the angle of the exoskeleton joint q_6.

References

[1] A. Pollock *et al.*, "Physical rehabilitation approaches for the recovery of function and mobility following stroke," *Cochrane Database Syst. Rev.*, vol. 4, 2014, Art. no. CD001920.

[2] F. J. Carod-Artal, D. S. Trizotto, L. F. Coral, and C. M. Moreira, "Determinants of quality of life in Brazilian stroke survivors," *J. Neurol. Sci.*, vol. 284, nos. 1–2, pp. 63–68, Sep. 2009.

[3] J. K. Freburger, D. M. Li, A. M. Johnson, and E. P. Fraher, "Physical and occupational therapy from the acute to community setting after stroke: Predictors of use, continuity of care, and timeliness of care," *Arch. Phys. Med. Rehabil.*, vol. 99, no. 6, pp. 1077–1089, 2018.

[4] C. D. Takahashi, L. Der-Yeghiaian, V. Le, R. R. Motiwala, and S. C. Cramer, "Robot-based hand motor therapy after stroke," *Brain*, vol. 131, pp. 425–437, Feb. 2008.

[5] R. Boian *et al.*, "Virtual reality-based post-stroke hand rehabilitation," *Stud. Health Technol. Inform.*, vol. 85, pp. 64–70, Feb. 2002.

[6] D. Popov, I. Gaponov, and J. H. Ryu, "Portable exoskeleton glove with soft structure for hand assistance in activities of daily living," *IEEE/ASME Trans. Mechatronics*, vol. 22, no. 2, pp. 865–875, Apr. 2017.

[7] A. Yurkewich, D. Hebert, R. H. Wang, and A. Mihailidis, "Hand extension robot orthosis (HERO) glove: Development and testing with stroke survivors with severe hand impairment," *IEEE Trans. Neural Syst. Rehabil. Eng.*, vol. 27, no. 5, pp. 916–926, May 2019.

[8] M. Cempini, M. Cortese, and N. Vitiello, "A powered finger–thumb wearable hand exoskeleton with self-aligning joint axes," *IEEE/ASME Trans. Mechatronics*, vol. 20, no. 2, pp. 705–716, Apr. 2015.

[9] M. Cempini, S. M. M. de Rossi, T. Lenzi, N. Vitiello, and M. C. Carrozza, "Self-alignment mechanisms for assistive wearable robots: A kinetostatic compatibility method," *IEEE Trans. Robot.*, vol. 29, no. 1, pp. 236–250, Feb. 2013.

[10] J. T. Li, R. Y. Zheng, Y. R. Zhang, and J. C. Yao, "iHandRehab: An interactive hand exoskeleton for active and passive rehabilitation," in *Proc. IEEE Int. Conf. Rehabil. Robot.*, Zurich, Switzerland, Jul. 2011, pp. 1–6.

[11] M. B. Hong, S. J. Kim, Y. S. Ihn, G.-C. Jeong, and K. Kim, "KULEX-hand: An underactuated wearable hand for grasping power assistance," *IEEE Trans. Robot.*, vol. 35, no. 2, pp. 420–432, Apr. 2019.

[12] D. Wang, Q. Meng, Q. Meng, X. Li, and H. Yu, "Design and development of a portable exoskeleton for hand rehabilitation," *IEEE Trans. Neural Syst. Rehabil. Eng.*, vol. 26, no. 12, pp. 2376–2386, Dec. 2018.

[13] N. S. K. Ho *et al.*, "An EMG-driven exoskeleton hand robotic training device on chronic stroke subjects: Task training system for stroke rehabilitation," in *Proc. IEEE Int. Conf. Rehabil. Robot.*, Zurich, Switzerland, Aug. 2011, pp. 1–5.

[14] I. Jo, Y. Park, J. Lee, and J. Bae, "A portable and spring-guided hand exoskeleton for exercising flexion/extension of the fingers," *Mech. Mach. Theory*, vol. 135, pp. 176–191, May 2019.

[15] M. Sarac, M. Solazzi, E. Sotgiu, M. Bergamasco, and A. Frisoli, "Design and kinematic optimization of a novel underactuated robotic hand exoskeleton," *Meccanica*, vol. 52, no. 3, pp. 749–761, Feb. 2017.

[16] R. A. Bos, K. Nizamis, B. F. J. M. Koopman, J. L. Herder, M. Sartori, and D. H. Plettenburg, "A case study with symbihand: An sEMG-controlled electrohydraulic hand orthosis for individuals with duchenne muscular dystrophy," *IEEE Trans. Neural Syst. Rehabil. Eng.*, vol. 28, no. 1, pp. 258–266, Jan. 2020.

[17] C. J. Nycz, T. Bützer, O. Lambercy, J. Arata, G. S. Fischer, and R. Gassert, "Design and characterization of a lightweight and fully portable remote actuation system for use with a hand exoskeleton," *IEEE Robot. Autom. Lett.*, vol. 1, no. 2, pp. 976–983, Jul. 2016.

[18] L. A. Legg, S. R. Lewis, O. J. Schofield-Robinson, A. Drummond, and P. Langhorne, "Occupational therapy for adults with problems in activities of daily living after stroke," *Stroke*, vol. 48, no. 11, pp. 321–322, Nov. 2017.

[19] Y. Di, Z. Han, and J. Ma, "Effect of occupational therapy on upper extremity function in stroke patients," *Chin. J. Rehabil.*, vol. 26, no. 3, pp. 188–189, 2011.

[20] N. Petroff, K. D. Reisinger, and P. A. Mason, "Fuzzy-control of a hand orthosis for restoring tip pinch, lateral pinch, and cylindrical prehensions to patients with elbow flexion intact," *IEEE Trans. Neural Syst. Rehabil. Eng.*, vol. 9, no. 1, pp. 225–231, Jun. 2001.

[21] P. Agarwal, J. Fox, M. K. O'Malley, A. D. Deshpande, and Y. Yun, "An index finger exoskeleton with series elastic actuation for rehabilitation: Design, control and performance characterization," *Int. J. Robot. Res.*, vol. 34, no. 14, pp. 1747–1772, Oct. 2015.

[22] A. Chiri, N. Vitiello, F. Giovacchini, S. Roccella, F. Vecchi, and M. C. Carrozza, "Mechatronic design and characterization of the index finger module of a hand exoskeleton for post-stroke rehabilitation," *IEEE/ASME Trans. Mechatronics*, vol. 17, no. 5, pp. 884–894, Oct. 2011.

[23] S. Ueki *et al.*, "Development of a hand-assist robot with multi-degrees-of-freedom for rehabilitation therapy," *IEEE/ASME Trans. Mechatronics*, vol. 17, no. 1, pp. 136–146, Feb. 2012.

[24] A. Wege and G. Hommel, "Development and control of a hand exoskeleton for rehabilitation of hand injuries," in *Proc. IEEE/RSJ Int. Conf. Intell. Robots Syst.*, Edmonton, AB, Canada, Aug. 2005, pp. 3046–3051.

[25] M. Cempini *et al.*, "Kinematics and design of a portable and wearable exoskeleton for hand rehabilitation," in *Proc. IEEE 13th Int. Conf. Rehabil. Robot. (ICORR)*, Seattle, WA, USA, Jun. 2013, pp. 1–6.

[26] J. M. Moran, J. H. Hemann, and A. S. Greenwald, "Finger joint contact areas and pressures," *J. Orthopaedic Res.*, vol. 3, no. 1, pp. 49–55, 1985.

[27] O. A. van Nierop, A. van der Helm, K. J. Overbeeke, and T. J. P. Djajadiningrat, "A natural human hand model," *Vis. Comput.*, vol. 24, no. 1, pp. 31–44, Nov. 2007.

[28] K.-C. Lin, P.-C. Huang, Y.-T. Chen, C.-Y. Wu, and W.-L. Huang, "Combining afferent stimulation and mirror therapy for rehabilitating motor function, motor control, ambulation, and daily functions after stroke," *Neurorehabil. Neural Repair*, vol. 28, no. 2, pp. 153–162, Feb. 2014.

[29] J. Kein, S. J. Spencer, and D. J. Reinkensmeyer, "Breaking it down is better: Haptic decomposition of complex movements aids in robot-assisted motor learning," *IEEE Trans. Neural Syst. Rehabil. Eng.*, vol. 20, no. 3, pp. 268–275, May 2012.

[30] D. G. Kamper, E. G. Cruz, and M. P. Siegel, "Stereotypical fingertip trajectories during grasp," *J. Neurophysiol.*, vol. 90, no. 6, pp. 3702–3710, 2003.

[31] M. Sarac, M. Solazzi, and A. Frisoli, "Design requirements of generic hand exoskeletons and survey of hand exoskeletons for rehabilitation, assistive, or haptic use," *IEEE Trans. Haptics*, vol. 12, no. 4, pp. 400–413, Oct. 2019.

[32] E. Y. Chao *et al.*, *Biomechanics of the Hand: A Basic Research Study*. Singapore: World Scientific, 1989.